



1 **Quantifying TOLNet Ozone Lidar Accuracy during the 2014**
2 **DISCOVER-AQ and FRAPPÉ Campaigns**

3

4 Lihua Wang¹, Michael J. Newchurch¹, Raul J. Alvarez II², Timothy A. Berkoff³, Steven S.
5 Brown², William Carrion^{3,4}, Russell J. De Young³, Bryan J. Johnson², Rene Ganoë⁴, Guillaume
6 Gronoff^{3,4}, Guillaume Kirgis^{2,5}, Shi Kuang¹, Andrew O. Langford², Thierry Leblanc⁶, Erin E.
7 McDuffie^{2,5,7}, Thomas J. McGee⁸, Denis Pliutau⁴, Christoph J. Senff^{2,5}, John T. Sullivan⁸, Grant
8 Sunnicht⁴, Laurence W. Twigg⁴, Andrew J. Weinheimer⁹

9

10 ¹University of Alabama in Huntsville, Huntsville, Alabama, USA

11 ²NOAA Earth System Research Laboratory, Boulder, Colorado, USA

12 ³NASA Langley Research Center, Hampton, Virginia, USA

13 ⁴Science Systems and Applications Inc., Lanham, Maryland, USA

14 ⁵Cooperative Institute for Research in Environmental Sciences, University of Colorado, Boulder, Colorado, USA

15 ⁶Jet Propulsion Laboratory, California Institute of Technology, Wrightwood, California, USA

16 ⁷Department of Chemistry, University of Colorado, Boulder, Colorado, USA

17 ⁸NASA Goddard Space Flight Center, Greenbelt, Maryland, USA

18 ⁹National Center for Atmospheric Research, Boulder, USA

19

20 Correspondence to Shi Kuang (kuang@nsstc.uah.edu)

21



22 Abstract

23 The Tropospheric Ozone Lidar Network (TOLNet) is a unique network of lidar systems that measure high-
24 resolution atmospheric profiles of ozone. The accurate characterization of these lidars is necessary to determine the
25 uniformity of cross-instrument calibration. From July to August 2014, three lidars, the TROPospheric OZone
26 (TROPOZ) lidar, the Tunable Optical Profiler for Aerosol and oZone (TOPAZ) lidar, and the Langley Mobile
27 Ozone Lidar (LMOL), of TOLNet participated in the “Deriving Information on Surface conditions from Column
28 and Vertically Resolved Observations Relevant to Air Quality” (DISCOVER-AQ) mission and the “Front Range Air
29 Pollution and Photochemistry Experiment” (FRAPPÉ) to measure ozone variations from the boundary layer to the
30 top of the troposphere. This study presents the analysis of the intercomparison between the TROPOZ, TOPAZ, and
31 LMOL lidars, along with comparisons between the lidars and other *in situ* ozone instruments including ozonesondes
32 and a P-3B airborne chemiluminescence sensor. In terms of the range-resolving capability, the TOLNet lidars
33 measured vertical ozone structures with an accuracy generally better than $\pm 15\%$ within the troposphere. Larger
34 differences occur at some individual altitudes in both the near-field and far-field range of the lidar systems, largely
35 as expected. In terms of column average, the TOLNet lidars measured ozone with an accuracy better than $\pm 5\%$ for
36 both the intercomparison between the lidars and between the lidars and other instruments. These results indicate
37 very good measurement accuracy for these three TOLNet lidars, making them suitable for use in air quality, satellite
38 validation, and ozone modeling efforts.

39 1. Introduction

40 1.1 TOLNet

41 The Tropospheric Ozone Lidar Network (TOLNet) provides time-height measurements of ozone from the
42 planetary boundary layer (PBL) to the top of the troposphere at multiple locations for satellite validation, model
43 evaluation, and scientific research (Newchurch et al., 2016; <http://www-air.larc.nasa.gov/missions/TOLNet/>).
44 Particularly, these high-fidelity ozone measurements can serve to validate NASA’s first Earth Venture Instrument
45 mission, Tropospheric Emissions: Monitoring Pollution (TEMPO), planned to launch in 2019. A second objective of
46 TOLNet is to identify a brassboard ozone lidar instrument that would be suitable to populate a network to address an
47 increasing desire for ozone profiles by air-quality scientists and managers within the modeling and satellite
48 communities (Bowman, 2013).

49 TOLNet consists of five ozone lidars across the United States and one in Canada: the Table Mountain
50 tropospheric ozone differential absorption lidar (DIAL) at NASA’s Jet Propulsion Laboratory, the Tunable Optical
51 Profiler for Aerosol and oZone (TOPAZ) lidar at NOAA’s Earth System Research Laboratory (ESRL), the Rocket-
52 city Ozone (O_3) Quality Evaluation in the Troposphere (RO₃QET) lidar at the University of Alabama in Huntsville
53 (UAH), the TROPospheric OZone (TROPOZ) DIAL at NASA’s Goddard Space Flight Space Center (GSFC), the
54 Langley Mobile Ozone Lidar (LMOL) at NASA’s Langley Research Center (LaRC), and Autonomous Mobile
55 Ozone Lidar Instrument for Tropospheric Experiments (AMOLITE) at Environment and Climate Change Canada.



56 All TOLNet lidars have unique configurations that are associated with their original measurement design
57 purposes, including their transmitter, receiver, and signal processing systems. Most components of these lidars are
58 customized and differ significantly in pulse energy, repetition rate, receiver size, solar (or narrow-band) interference
59 filter, and range resolution. These differences result in varying signal-to-noise ratios (SNRs), which impact the
60 useful operating ranges and statistical uncertainties in ozone retrieval. The selection of the DIAL wavelengths
61 determines the sensitivity to interference by other species, primarily aerosols. In addition, multiple lidar data
62 processing and retrieval algorithms could also lead to different effective resolutions and lidar retrieval uncertainties
63 (Godin et al., 1999; Leblanc et al., 2016). Therefore, it is important to quantify the measurement differences between
64 the TOLNet lidars and understand their sources before we form a consistent TOLNet dataset. A previous
65 intercomparison between TROPOZ and LMOL reported by Sullivan et al. (2015) concluded that the observed ozone
66 column averages from the two lidars were within $\pm 8\%$ of each other, and their ozone profiles were mostly within
67 $\pm 10\%$ of each other. That particular study served as the first reported measurement intercomparison of two ground-
68 based tropospheric ozone lidar systems within the United States.

69 1.2 DISCOVER-AQ 2014 and FRAPPÉ Campaigns

70 The scientific goal of the TOLNet lidars in this study was to provide continuous, high-resolution
71 tropospheric ozone profiles to support the NASA-sponsored DISCOVER-AQ mission
72 (<https://www.nasa.gov/larc/2014-discoveraq-campaign/>), and the National Science Foundation (NSF) and state of
73 Colorado (CO) jointly sponsored FRAPPÉ (Dingle et al., 2016) from July to August 2014. By collaborating with
74 FRAPPÉ, the 2014 CO study was the final stop in a series of four field campaigns by DISCOVER-AQ to understand
75 sources, transport and chemical transformations of air pollutants, particularly those that lead to ground-level ozone
76 formation (Crawford and Pickering, 2014).

77 Prior to the two campaigns, TOPAZ, TROPOZ, and LMOL were all deployed to the same location in Erie,
78 CO to obtain intercomparison data at the Boulder Atmospheric Observatory (BAO) (40.050°N, 105.003°W, 1584 m
79 above sea level, ASL). Subsequent to the BAO intercomparison, TROPOZ and LMOL re-deployed to locations near
80 Fort Collins, CO (~60 km north-northwest of BAO) and Golden, CO (~40 km southwest of BAO), respectively, for
81 their different scientific missions. During the DISCOVER-AQ and FRAPPÉ campaigns, balloon-borne ozonesondes
82 were launched at selective sites. In addition, the NASA P-3B aircraft performed multiple spiral ascents and descents
83 over several ground sites and provided numerous vertical profiles of ozone measurements. In this study, we compare
84 retrievals between the three lidars and evaluate the ozone lidar accuracy using ozonesonde and P-3B aircraft
85 measurements. These two campaigns offered a unique opportunity for the lidar validation work, as they involved so
86 many different instruments.

87 2. Instruments

88 2.1 TOLNet Lidars



89 **Table 1** lists the main hardware specifications of the three TOLNet lidars and their ozone retrieval
90 processes, which could potentially impact the intercomparison result.

91 2.1.1 TROPOZ/NASA GSFC

92 The transmitter for TROPOZ consists of two 50-Hz Nd:YAG- lasers used to pump two Raman cells filled
93 with Deuterium (D₂) and Hydrogen (H₂) gases, respectively, to generate two outgoing lasers at 289 and 299 nm. The
94 typical pulse energies are 12 mJ at 299 nm (off-line) and 16 mJ at 289 nm (on-line) (Sullivan et al., 2014). The
95 receiving system consists of a 45-cm-diameter Newtonian telescope for measuring far field and four smaller 2.5-cm
96 refracting telescopes to measure near field. The 45-cm telescope has a 1-mrad field of view (FOV), and the 2.5-cm
97 telescopes have a much wider FOV at 10 mrad. In each channel, solar interference filters with a 1-nm bandwidth
98 decrease the amount of ambient solar light, which improves the SNR. The fundamental range resolution for the data
99 acquisition system is 15 m (100 ns). TROPOZ measures ozone up to 16 km during daytime hours and higher
100 altitudes at night.

101 2.1.2 TOPAZ/NOAA ESRL

102 The TOPAZ lidar is a truck-mounted zenith-looking, scanning instrument modified from the nadir-looking
103 airborne DIAL configuration first used in the 2006 Texas Air Quality Study (TexAQ5 II) (Alvarez et al., 2011;
104 Senff et al., 2010). The lidar transmitter is based on a Ce:LiCAF laser pumped by a quadrupled Nd:YLF laser to
105 produce three UV wavelengths, each at a 333 Hz repetition rate and tunable from 283 nm to 310 nm. The actual
106 wavelengths used during DISCOVER-AQ 2014 were 287, 291, and 294 nm. Compared to the conventional two-
107 wavelength DIAL, the three-wavelength configuration can potentially minimize the aerosol interference by using the
108 dual-DIAL retrieval technique (Kovalev and Bristow, 1996) without assuming a lidar ratio and Angström exponent.
109 However, in this study, ozone was retrieved using the 287- and 294-nm lidar signals and the standard two-
110 wavelength DIAL algorithm because the two-wavelength retrieval was less affected by significant lidar signal noise
111 (Alvarez et al., 2011).

112 Laser light backscattered by air molecules and aerosol particles is collected with a co-axial 50-cm diameter
113 Newtonian telescope and then split at a 1:9 ratio into near- and far-field detection channels. The FOVs of the near-
114 and far-field channels are controlled by different-size apertures resulting in full overlap at distances of ~300 m and
115 ~800 m, respectively. Both channels use gated photomultipliers (PMTs) operated in analog mode with solar
116 interference filters during the daytime. Compared to photon counting (PC) signals, the analog signal is able to keep
117 high linearity for strong signals and is particularly suitable for near-range measurement. The two-axis scanner on the
118 truck permits pointing the laser beam at several shallow elevation angles at a fixed, but changeable azimuth angle,
119 typically at 2°, 6°, 20°, and 90° elevation angles that are repeated approximately every 5 minutes. The ozone profiles
120 at these four angles are spliced together to create composite vertical profiles extending from 10 m to about 2 km
121 AGL (Langford et al., 2016). The range resolution of the signal recording system is 6 m.

122 During the 2014 DISCOVER-AQ and FRAPPÉ campaigns, the TOPAZ ozone observations at low
123 elevation angles (2°, 6°, and 20°) suffered from a slight, but consistent range-dependent bias created by an unknown



124 source of noise in the data acquisition system. The cause of this noise remains unknown and attempts to correct the
125 resulting bias were unsuccessful. This bias manifests itself primarily in the low-angle observations because the
126 signal levels and SNR are significantly lower compared to the measurements at 90°. For these reasons, the low angle
127 observations below 500 m were excluded from the comparisons reported within this study.

128 **2.1.3 LMOL/NASA LaRC**

129 The transmitter of LMOL consists of a diode-pumped Nd:YLF laser pumping a Ce:LiCAF tunable UV
130 laser to obtain two wavelengths typically at 287.1 and 292.7 nm with a pulse energy of 0.2 mJ at 500 Hz for each
131 wavelength. The lidar receiver system consists of a 40-cm telescope with a 1.4-mrad FOV to measure far field and
132 another 30-cm telescope with an adjustable FOV to measure near field (De Young et al., 2017). The raw lidar
133 signals are recorded with a 7.5-m range resolution. The LMOL data acquisition system operates in both analog and
134 PC modes. In this study, LMOL measures ozone between 0.7 and 4.5 km. Ozone measurements for DISCOVER-AQ
135 represent LMOL's very first remote deployment.

136 **2.1.4 Lidar Data Processing and Retrieval Algorithms**

137 The data processing and DIAL retrieval algorithms for the three TOLNet lidars are similar but not identical.
138 Their details have been described by Alvarez et al. (2011), De Young et al. (2017), Langford et al. (2011), and
139 Sullivan et al. (2015; 2014). Some basic procedures were applied on the raw lidar signals before retrievals, such as
140 time integration (5 min for this study), dead-time correction (for PC only), background correction, merging of PC
141 and analog signals (for a system with both PC and analog channels), and signal-induced-bias (SIB) correction
142 (Kuang et al., 2013). Some parameters are system dependent or empirical due to different equipment, such as the
143 dead-time value, PC-analog timing offset, averaging range for background calculation, and SIB simulation function.
144 All groups agreed to use the Brion-Daumont-Maliget (BDM) database (Daumont et al., 1992; Maliget et al., 1995;
145 Brion et al., 1993) to calculate differential ozone absorption cross-sections, which are temperature-dependent.

146 The ozone number density profile results from computing the derivative of the logarithm of the on-line to
147 off-line signal ratios. Spatial smoothing is usually necessary to improve the SNR and reduce the statistical errors.
148 Various smoothing methods and their impacts on final lidar retrieval have been described by Godin et al. (1999).
149 Both TROPOZ and LMOL groups applied a Savitzky-Golay (SG) filter with a 2nd degree polynomial on the
150 derivative of the logarithm of the on-line to off-line signal ratios with an increasing window width to accommodate
151 the quickly decreasing SNR. However, the SG window sizes for TROPOZ and LMOL are different due to different
152 SNRs at each altitude. The TOPAZ group smoothed the derivative with a five-point least-square fitting in a 450-m
153 interval. The different retrieval methodologies and parameters affect the effective vertical resolution of the retrieved
154 ozone profiles, as listed in Table 1. This effective resolution determines the capability of the lidars to resolve vertical
155 ozone structure and is not equal to, but is associated with, the fitting window width.

156 All groups applied similar schemes to correct the aerosol interference. These schemes iteratively substitute
157 derived ozone from the DIAL equation into the lidar equation to solve aerosol extinction and backscatter until both
158 aerosol and ozone converge (Alvarez et al., 2011; Kuang et al., 2011; Sullivan et al., 2014). The differential aerosol



159 backscatter and extinction were calculated with the approximation from Browell et al. (1985). Lidars directly
160 measure the ozone number density, and all three groups used the same temperature and pressure profiles from co-
161 located ozonesonde measurements for Rayleigh correction, ozone mixing-ratio calculations, and computation of the
162 temperature dependent ozone absorption cross sections.

163 Merging between different altitude channels, either different telescopes or different optical channels of the
164 same telescope, is challenging with limited methodologies reported in the literature (Kuang et al., 2011). It is
165 difficult to specify a method for all groups because merging is system-dependent and is affected by many factors
166 previously described. Therefore, the three lidar groups merge the ozone profiles at different altitudes optimized for
167 their system and SNR levels such as the example method described by Sullivan et al. (2015). As a result, additional
168 differences between systems can occur due to the non-standardized altitude channel merging.

169 **2.1.5 Error budget of the lidar measurements**

170 Only a brief description of the error budget of the lidar measurements is provided in this paper since the
171 details have been discussed in the respective instrument paper (Alvarez et al., 2011; De Young et al., 2017; Sullivan
172 et al., 2014). Table 2 presents the estimated measurement uncertainties for 5 or 30-min integration time for the three
173 lidars. Statistical errors (Papayannis et al., 1990) arising from signal and background noise fluctuations are random
174 errors and may be improved by additional averaging or smoothing. The maximum statistical uncertainties for the
175 three lidars are similar (20% for 5 min and 8% for 30 min) within their measurable ranges although they are
176 different at the same altitude. The uncertainty arising from aerosol interference could be the largest systematic error
177 source and can be minimized by using the appropriate correction algorithm (Eisele and Trickl, 2005; Immler, 2003;
178 Sullivan et al., 2014). The estimated total lidar measurement uncertainties are 22% and 13% for 5 and 30 min,
179 respectively, within the lidar measurement ranges listed in Table 1.

180 **2.2 Ozonesondes**

181 An ozonesonde is a lightweight, balloon-borne instrument that consists of a Teflon air pump and an ozone
182 sensor interfaced to a meteorological radiosonde. The ozone sensor uses an electrode electrochemical cell containing
183 potassium iodide (KI) solution (Komhyr, 1969; Komhyr et al., 1995) to measure ozone with a precision better than
184 $\pm 5\%$ and an accuracy better than $\pm 10\%$ up to 35 km altitude with a sampling interval of about 1 s and a retrieval
185 vertical resolution of 100 m (Deshler et al., 2008; Johnson et al., 2008; Smit et al., 2007). The uncertainty of
186 ozonesonde measurement is larger in the troposphere than that in the stratosphere (Liu et al., 2009). As the balloon
187 carrying the instrument package ascends through the atmosphere, the pump bubbles ambient air into the sensor cell.
188 The reaction of ozone and iodide generates an electrical signal proportional to the amount of ozone. A radiosonde
189 attached in the same package measures air temperature, pressure, and relative humidity (Stauffer et al., 2014).
190 Ozonesondes are capable of measuring ozone under various weather conditions (e.g., cloudy, thunderstorm). The
191 free-flying ozonesondes typically reach 35-km altitude in less than two hours with a rise rate at about 5 m/s.



192 **2.3 Ozone Measurement Instrument onboard NASA's P-3B**

193 NASA's P-3B aircraft is a pressurized, four-engine turboprop, capable of long-duration flights of 8-12
194 hours and is based out of NASA's Wallops Flight Facility in Wallops Island, Virginia. A series of gas and aerosol
195 instruments were outfitted within the P-3B aircraft. Ozone was measured using the National Center for Atmospheric
196 Research (NCAR)'s 4-channel chemiluminescence instrument based on the reaction between ambient ozone and
197 nitric oxide (NO) with an accuracy of about $\pm 5\%$ and sampling interval of 1 s (Weinheimer et al., 1993; Ridley et
198 al., 1992). The precision of this ozone detector is better than $\pm 1\%$ when ambient ozone is higher than 10 ppbv. The
199 P-3B aircraft flew spirals from 300 m to 4570 m above the surface over selected ground monitoring sites including
200 all three lidar sites (more information in Section 3.3) during the DISCOVER-AQ 2014 campaign.

201 **3. Results**

202 **3.1 Lidar Intercomparisons**

203 The three TOLNet lidars were deployed next to the BAO tower to take simultaneous measurements before
204 the DISCOVER-AQ/FRAPPÉ campaign. They were only a few hundreds of meters away from each other and were
205 within 5 m of the same elevation (see measurement locations in Table 1).

206 Unlike stratospheric ozone lidars that focus on integrating hours of observations, tropospheric ozone lidars
207 need to detect ozone variations with timescales on the order of minutes, when considering ozone's shorter lifetime,
208 smaller-scale transport, and mixing processes within the PBL and free troposphere (Steinbrecht et al., 2009;
209 McDermid et al., 1990). Therefore, we processed all lidar data on a 5-min temporal scale (signal integration time).
210 Rayleigh correction was performed with the same atmospheric profile from the ozonesonde. Because the three lidars
211 have different fundamental range resolutions, retrieved ozone number density values were internally interpolated on
212 the same altitude grid with a 15-m interval for comparison.

213 Figure 1 presents the comparison of the TOPAZ and TROPOZ observed ozone at BAO from 1300 to 2135
214 UTC (6 hours ahead of local time, Mountain Daylight Time) on July 11, 2014 under a partly cloudy sky condition.
215 Data influenced by cloud interferences were filtered out. Ozone curtains from both lidars (Figure 1 a and b) show a
216 significant (about 40%) ozone increase in the early afternoon. A total of 7655 TOPAZ and TROPOZ coincident
217 pairs were constructed between 0.6 and 2 km AGL (altitude range over which both lidars provided valid data) over
218 this time period. The measurement differences between the two lidars are mostly within $\pm 5\%$ at individual grids
219 (Figure 1 c). The product of averaged ozone concentration over some specified altitude range can represent the
220 atmospheric ozone abundance and can be also useful for satellite validation. Here, we refer this product as ozone
221 column average with the unit of number density, not to be confused with integrated column ozone often reported in
222 Dobson units. The statistics of the intercomparison of the column averages is listed in Table 3. The similar 1σ
223 standard deviations (17.8 and $16.7 \times 10^{16} \text{ molec}\cdot\text{m}^{-3}$) suggest similar ozone variations captured by both lidars. The
224 mean relative difference (or normalized bias) was calculated by averaging the relative difference (i.e., (TROPOZ-
225 TOPAZ)/TOPAZ, the denominator was arbitrarily chosen) for all paired ozone profiles. The $-1.1 \pm 2.6\%$ mean



226 relative difference suggests excellent agreement of the averaged ozone column (Figure 1 d) for 80 profiles over 6.5
227 hours between TOPAZ and TROPOZ retrievals.

228 Figure 2 shows the TOPAZ-LMOL intercomparison for data taken on July 16, 2014 with 1902 coincident
229 pairs from 0.9 to 2 km and between 1340 to 1730 UTC on this day. Some of the data gaps were due to low clouds
230 blocking the lidar beams. The retrievals between the two lidars agree with each other mostly within $\pm 10\%$ (Figure 2
231 c). LMOL measured a mean ozone column average (Figure 2 d) $3.8 \pm 2.9\%$ lower than TOPAZ for a total of 28
232 paired profiles, which is significantly fewer than those from the TROPOZ-TOPAZ comparison.

233 The generally random distribution of the relative differences in Figure 1 (c) and 2 (c) suggests overall
234 consistent measurements with small systematic errors from all three lidars. In summary, TROPOZ, LMOL, and
235 TOPAZ report ozone values at individual altitudes mostly within $\pm 10\%$, which is well within their respective
236 uncertainties and report ozone column averages within $\pm 3.8\%$ on average.

237 3.2 Lidars versus Ozonesondes

238 In order to compare the lidar data to ozonesondes, the Rayleigh- and aerosol-corrected lidar data was
239 converted from ozone number densities to ozone mixing ratios by using sonde-measured pressure and temperature
240 profiles, and averaged over a 30-minute interval (± 15 minutes around sonde launch times). The ozonesondes report
241 values approximately every second (about every 5 m in altitude) in raw data. For comparison, the ozonesonde raw
242 data were linearly interpolated on the lidar altitude grids with a 15-meter interval. Figure 3 shows the mean ozone
243 mixing ratios measured by TOLNet lidars and ozonesondes, as well as their mean relative difference as function of
244 altitude.

245 After the DISCOVER-AQ/FRAPPÉ campaign started, the TROPOZ lidar deployed to Fort Collins, CO to
246 measure ozone. There were 11 ozonesonde profiles that were coincident and co-located with the TROPOZ
247 measurements. The mean ozone profiles of TROPOZ and sondes (Figure 3a) show similar vertical variations with
248 enhanced PBL and upper tropospheric ozone. The mean relative differences between TROPOZ and ozonesondes
249 (Figure 3b) are mostly within $\pm 10\%$ up to 9 km. The local maximum of the differences at 1.8 km is associated with
250 the merging of ozone retrievals from the near-field channel and far-field channel. Above 9 km, the biases start to
251 increase and exceed 25% with large oscillations due to large statistical errors as a consequence of low SNR. Biases
252 between 10-20% are still very representative of the upper free troposphere. On average for altitudes from 0.35 to 12
253 km, TROPOZ measures 2.9% higher ozone than the ozonesondes. This difference can be seen as the mean
254 difference of ozone column average between the ozonesondes and lidar for a 30-min integration time.

255 Between July 10 and July 16, a total of 10 ozonesondes were released near the BAO tower and 7 of them
256 were coincident with TOPAZ measurements (3 on July 10, 3 on July 11, and 1 on July 16). TOPAZ mostly agrees
257 with ozonesondes between -5% and 10% (Figure 3 c, d). Compared to ozonesondes, TOPAZ measures 4.4% more
258 PBL ozone on average.

259 On July 16, there was only one pair of coincident LMOL and ozonesonde measurements at the BAO tower
260 (Figure 3 e, f). The 30-minute averaged LMOL ozone profile agrees with the ozonesonde mostly within 0-15%



261 between 0.95 and 4.5 km AGL with an overall average of 6.2%. The maximum bias occurring at far range (above 4
262 km) is principally due to low SNR. The bias observed at 1.5 km is likely due to the high variation in aerosol
263 concentration, that was also observed in the green channel. Since there is only one comparison between the LMOL
264 and ozonesonde, the statistical information on the overall bias between their measurements is not available.

265 In summary, all three TOLNet lidars exhibit overall positive bias, up to 4.4%, compared to ozonesondes
266 excluding the single profile comparison to LMOL (6.2%). The larger bias than the climatological difference
267 between lidar and ozonesondes reported by Gaudel et al. (2015) (0.6 ppbv) could be associated with the much
268 shorter averaging time period. The maximum biases exist in two regions, near-range altitudes and far-range
269 altitudes. The large far-range bias is expected and is primarily associated with the high statistical errors arising from
270 low SNR. The large near-range bias is more complicated and could be associated with various factors, primarily the
271 aerosol correction and the merging of signal or ozone from different optical or altitude channels.

272 3.3 Lidars versus P-3B Chemiluminescence Instrument

273 During the campaigns, the P-3B aircraft measured ozone profiles while doing spirals above the lidar sites.
274 There are 34 coincident profiles between TROPOZ and the P-3B at Fort Collins, 29 between TOPAZ and the P-3B
275 at the BAO tower, and 9 between LMOL and the P-3B at Golden, CO. The distances between the lidar and P-3B
276 spiral centers for these paired profiles were less than 11 km. To make coincident pairs between P-3B and lidar data,
277 we interpolate the P-3B data onto the lidar vertical grids with a 15-m vertical resolution. Figure 4 shows the average
278 ozone profiles measured by the lidars and the P-3B as well as their mean relative differences. TROPOZ and the P-
279 3B agree with each other within $\pm 5\%$ between 0.5 to 3.5 km (Figure 4 a, b) with a -0.8% overall average relative
280 difference. TOPAZ agrees with the P-3B within -11% and 3% between 0.5 and 2 km (Figure 4 c, d) with a -2.7%
281 overall average relative difference. TOPAZ underestimates the lower-PBL (<1.5 km) ozone compared to P-3B, but
282 when compared to ozonesondes TOPAZ overestimates ozone at many of these same altitudes (see Figure 3 d).
283 LMOL agrees with P-3B mostly within -5% and 0% above 1800 m and within -15% and -5% between 0.7-1.8 km
284 (Figure 4 e, f) with a -4.9% overall average relative difference.

285 In summary, TOPAZ and LMOL exhibited noticeable negative bias in the PBL compared to the P-3B while
286 TROPOZ measured slightly lower than the P-3B. The differences between the two lidars and the P-3B are not
287 significantly correlated suggesting that the problem was not likely from the P-3B ozone instrument. These
288 differences could at least in part be caused by the lidar systematic errors mentioned in Section 2.1.5, but could also
289 reflect horizontal ozone variability across the P-3B spirals, which were up to 22 km in diameter.

290 4. Summary and Conclusions

291 Intercomparisons have been made between three of the six TOLNet ozone lidars (NASA GSFC's
292 TROPOZ, NOAA ESRL's TOPAZ, and NASA LaRC's LMOL) and between the lidars and other *in situ* ozone
293 measurement instruments using coincident data during the 2014 DISCOVER-AQ and FRAPPÉ campaigns at
294 NOAA's BAO in Erie, CO. On average, TROPOZ, TOPAZ, and LMOL reported very similar ozone within their
295 reported uncertainties for a 5-min signal integration time. The three lidars measured consistent ozone variations



296 revealed in the lidar time-height curtains and in the distribution of their relative differences. From intercomparisons
297 between the lidars and other instruments we find (1) All lidars measure higher ozone than ozonesondes with an
298 averaged relative difference within 4.4%. The lidar profile measurements agree with the ozonesonde observations
299 within -10-15% in their measurable ranges except at a few near-field altitudes. These results are generally consistent
300 with Sullivan et al. (2015) from a similar ozonesonde-lidar intercomparison. (2) TROPOZ agrees with the P-3B
301 chemiluminescence Instrument below 3.5 km within $\pm 5\%$ with a small column-averaged relative difference of -
302 0.8%. TOPAZ and LMOL exhibit a slightly larger bias mostly between -15% and 5% below 2 km compared to P-3B
303 with a column-averaged difference of -2.7% and -4.9%, respectively.

304 Overall, intercomparisons between themselves and with *in situ* instruments suggest that the TOLNet lidars
305 are capable of capturing high-temporal tropospheric-ozone variability and measuring tropospheric ozone with
306 accuracy better than $\pm 15\%$ in terms of their vertical resolving capability and better than $\pm 5\%$ in terms of their
307 column measurement. These lidars have sufficient accuracy for model evaluation and satellite validation (Liu et al.,
308 2010). Since the 2014 campaigns, the TOLNET lidars have been modified to improve their stability and their
309 accuracy. The validation of these upgraded lidars will be reported in a future paper.

310 **Acknowledgement**

311 This work is supported by the TOLNet program developed by the National Aeronautics and Space
312 Administration (NASA)'s Science Mission Directorate and by the National Oceanic and Atmospheric
313 Administration Earth System Research Laboratory. Dr. John T. Sullivan's research was supported by an
314 appointment to the NASA Postdoctoral Program at the NASA Goddard Space Flight Center, administered by
315 Universities Space Research Association under contract with NASA. The views, opinions, and findings contained in
316 this report are those of the authors and should not be construed as an official NOAA, NASA, or U.S. Government
317 position, policy, or decision.

318



319

Table 1. Specifications for the TOLNet lidars.

	TROPOZ	TOPAZ	LMOL
Transmitter			
Laser type	Nd:YAG pumped D ₂ , H ₂ Raman cell	Nd:YLF pumped Ce:LiCAF	Nd:YLF pumped Ce:LiCAF
Wavelengths (nm)	288.9, 299.1	287, 291, 294	287.1, 292.7
Pulse Repetition Rate (Hz)	50	333	500
Pulse energy (mJ)	12 (299 nm), 16 (289 nm)	~0.06 for all wavelengths	0.2 for both wavelengths
Detection and data acquisition system			
Telescope diameter (cm)	45, 2.5	50	40, 30
FOV (mrad)	1 (45 cm), 10 (2.5 cm)	1.5 (far field channel), 3 (near field channel)	1.4 (far field channel), variable FOV (near field channel)
Signal detection type	PMT	PMT	PMT
Data acquisition type	PC	Analog	Analog and PC
Fundamental range resolution (m)	15	6	7.5
Instrument reference	(Sullivan et al., 2014)	(Alvarez et al., 2011)	(DeYoung et al., 2017)
DIAL retrieval			
DIAL retrieval and smoothing method	1 st -order (differential) SG filter with a 2 nd degree polynomial with an increasing window width applied on the derivative of the logarithm of the signal ratios	five-point least square fitting with a 450-m window applied on the derivative of the logarithm of the signal ratios	1 st -order (differential) SG filter with a 2 nd degree polynomial, with an increasing window width applied on the derivative of the logarithm of the signal ratios
Retrieval effective resolution (m)	~100 at 1 km degrading to ~800 at 10 km	~10 below 50 m, ~30 from 50 to 150 m, ~100 from 150 to 500 m, 315 above 500 m	225 below 3 km degrading to 506 above 3 km
Aerosol correction reference	(Kuang et al., 2011; Sullivan et al., 2014)	(Alvarez et al., 2011)	(Browell et al., 1985; DeYoung et al., 2017)
Valid altitudes (km above ground level, AGL)	0.35-16	0.01-2	0.7-4.5
Measurement location			
Latitude (°N)	40.050	40.045	40.050
Longitude (°W)	105.000	105.006	105.004
Elevation (m ASL)	1584	1587	1584

320

321



322 **Table 2. Estimated uncertainties for TROPOZ, TOPAZ and LMOL ozone measurements within their measurable range**
 323 **(see Table 1) for the 5 or 30-min integration time.**

Source	Uncertainty	
	5-min integration	30-min integration
Statistical error	<20%	<8%
Aerosol interference	<10%	
Interference by SO ₂ , NO ₂ , O ₂ dimmer	<1.5%	
Differential Rayleigh scattering	<1%	
Total*	<22%	13%

324 *Total root-mean-square error.

325

326

327

328

329

330

331

332

333

334

335

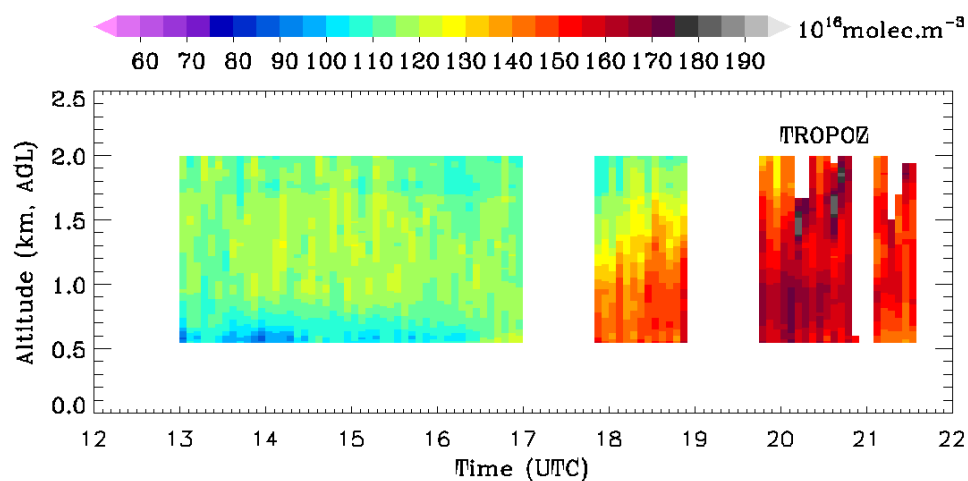
336

Table 3. Comparisons of the ozone column average measured by TROPOZ, TOPAZ, and LMOL.

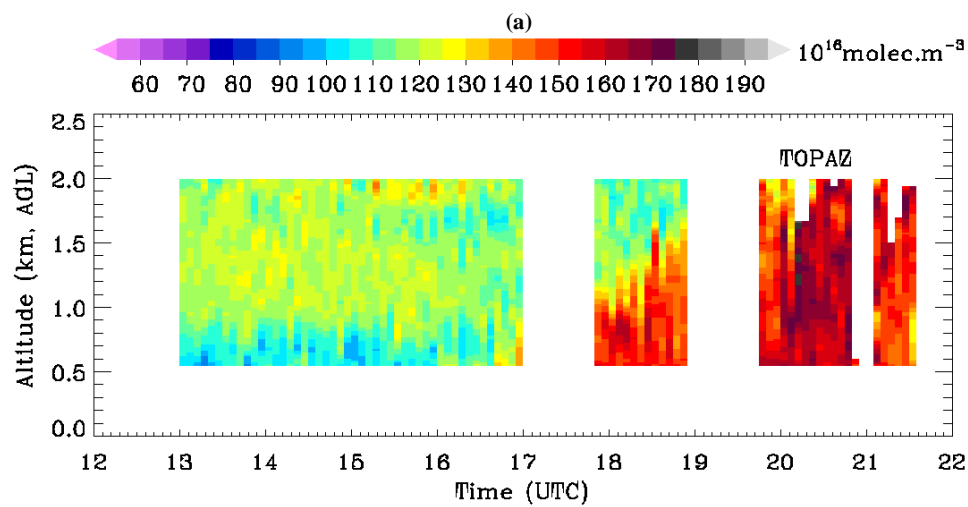
Date	UTC time range	Altitude range (km)	Lidar	Number of the paired profiles	Mean ozone column average (10 ¹⁶ molec·m ⁻³)	1σ of the ozone column average (10 ¹⁶ molec·m ⁻³)	Mean relative difference *	1σ of the difference
7/11/2014	1300 - 2135	0.6-2	TROPOZ/ TOPAZ	80	127.3/128.6	17.8/16.7	-1.1%	2.6%
7/16/2014	1335 - 1730	0.9-2	LMOL/T OPAZ	28	98.1/102.0	13.1/13.0	-3.8%	2.9%

337 * Equal to mean (A-B)/B for A/B in 'Lidar' column for all paired profiles.

338



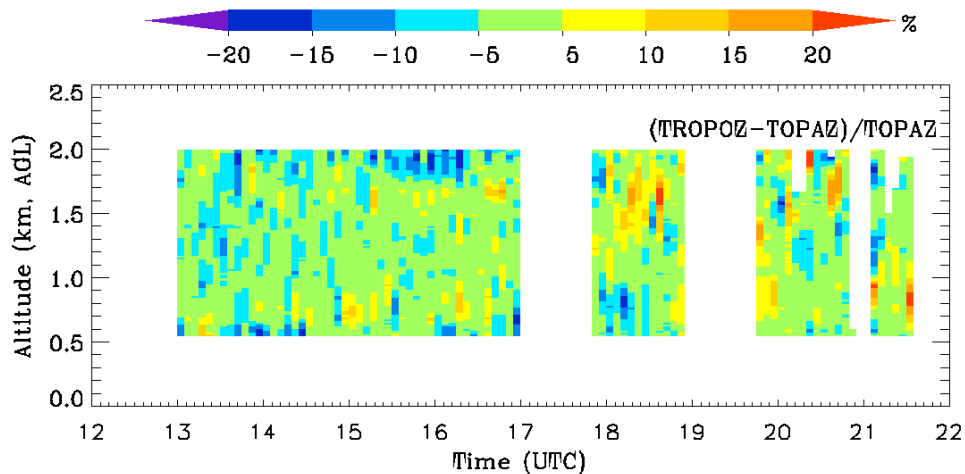
339
340



341
342



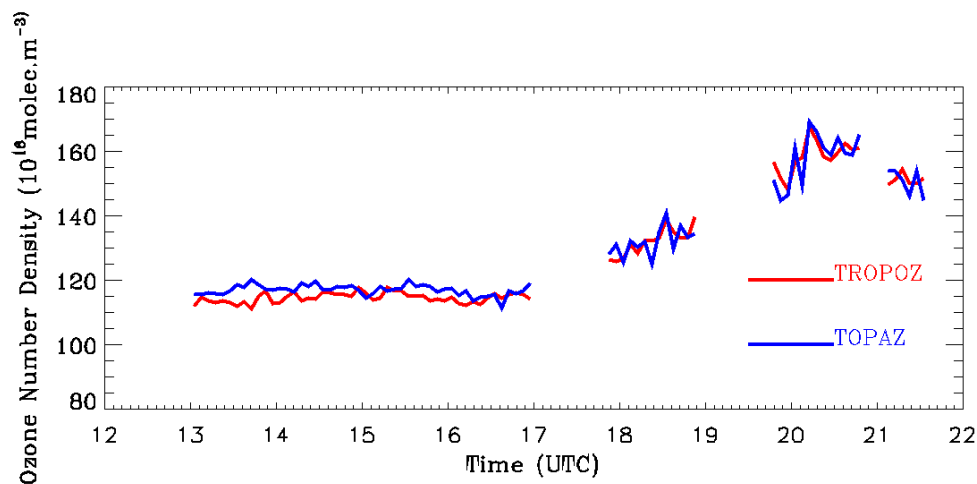
343



344

345

(c)



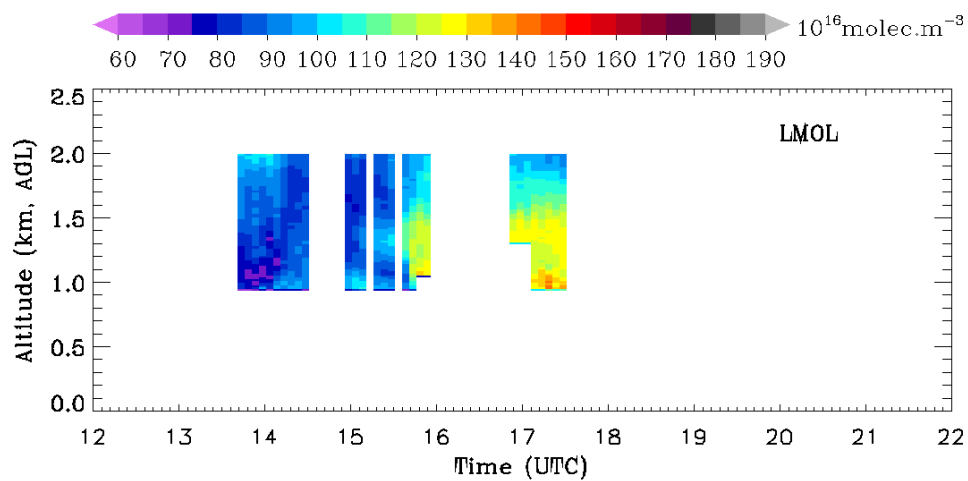
346

347

(d)

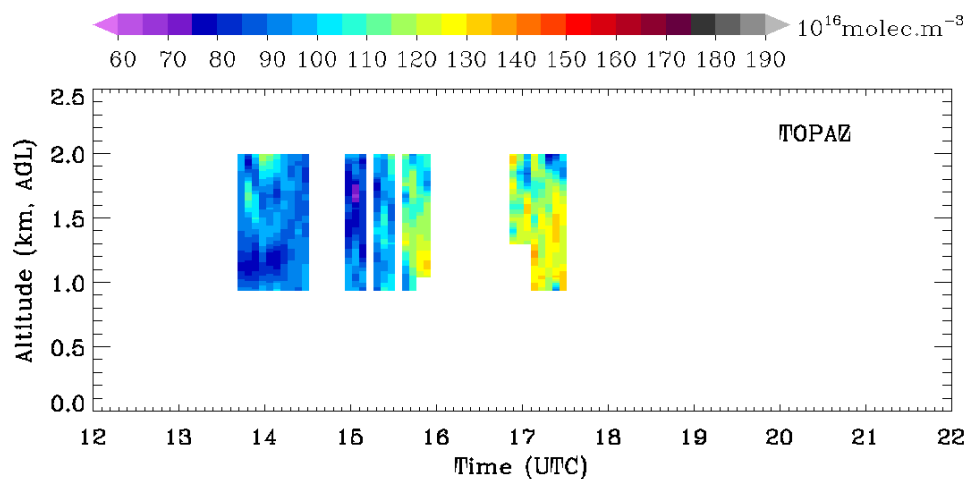
348 **Figure 1.** Comparisons of ozone measured by TROPOZ and TOPAZ. (a) Ozone number densities measured by TROPOZ.
349 (b) Ozone number densities measured by TOPAZ. (c) Their relative percent differences, $(\text{TROPOZ}-\text{TOPAZ})/\text{TOPAZ}$. (d)
350 Column averages measured by the TROPOZ and TOPAZ. TROPOZ measures $1.1\pm 2.6\%$ lower ozone column average
351 than TOPAZ.

352



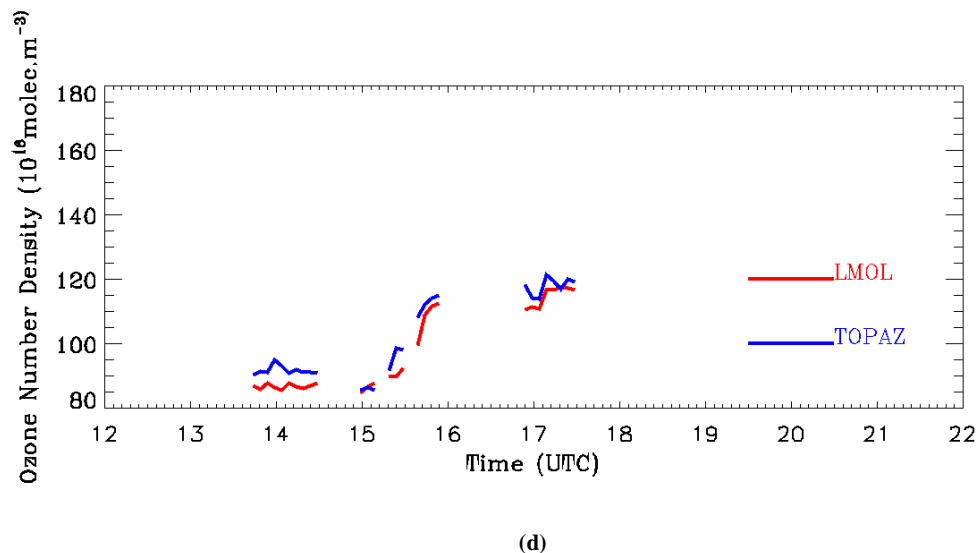
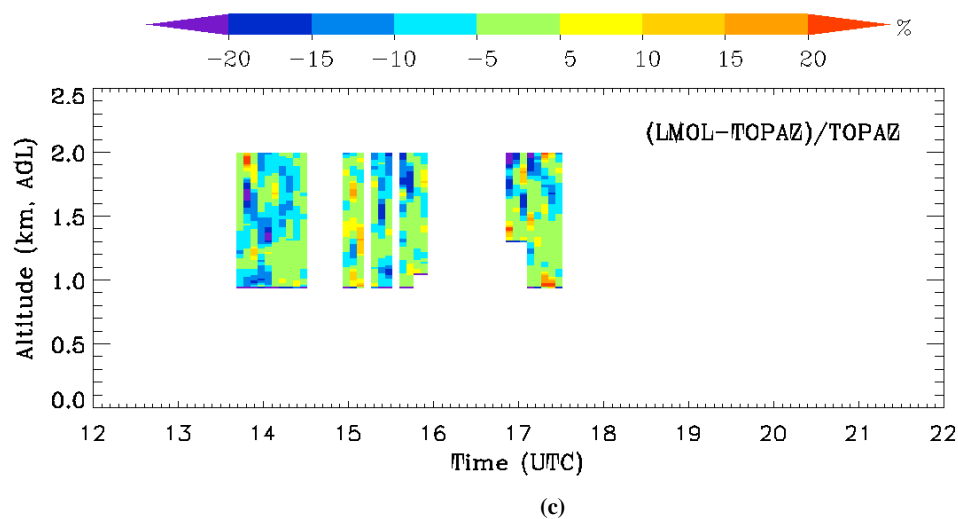
353
354

(a)



355
356

(b)

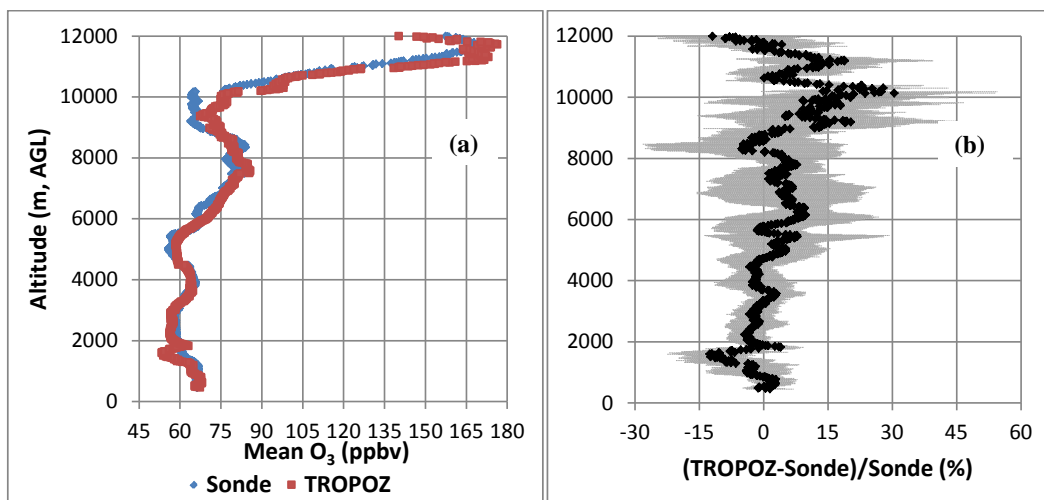


361 Figure 2. Comparisons of ozone measured by LMOL and TOPAZ. (a) LMOL-measured ozone number densities. (b)
362 TOPAZ-measured ozone number densities. (c) Their relative percent differences, $(\text{LMOL} - \text{TOPAZ}) / \text{TOPAZ}$. (d) Column
363 averages measured by LMOL and TOPAZ. LMOL measures $3.8 \pm 2.9\%$ lower ozone column average than TOPAZ.

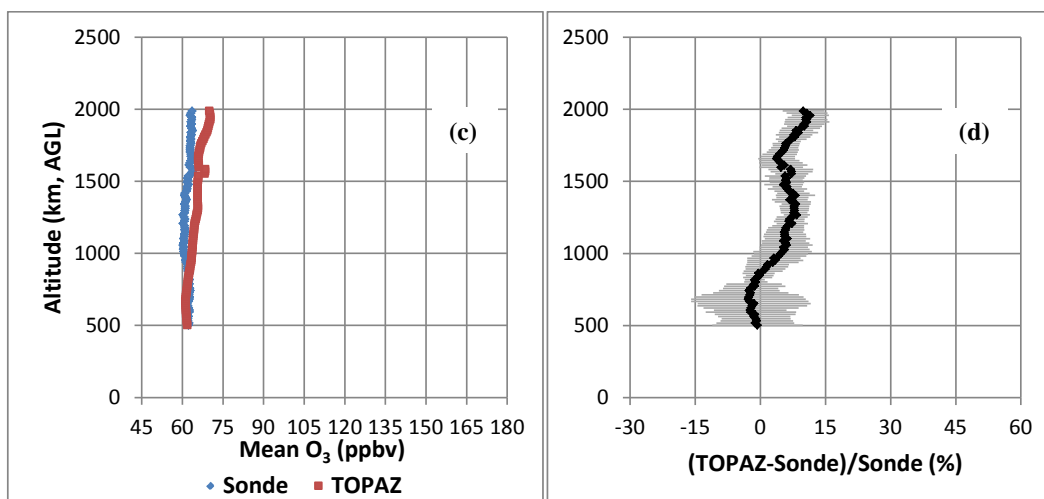
364

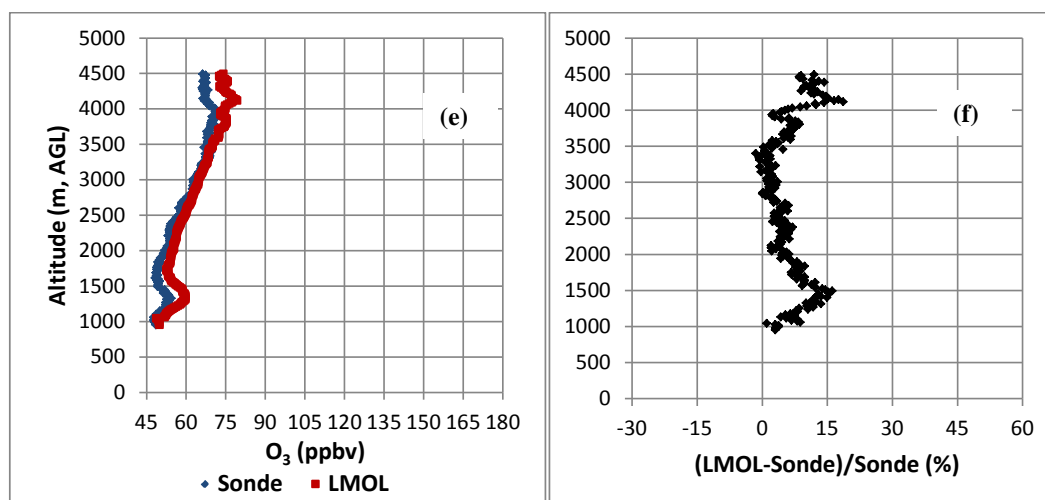


365



366





367

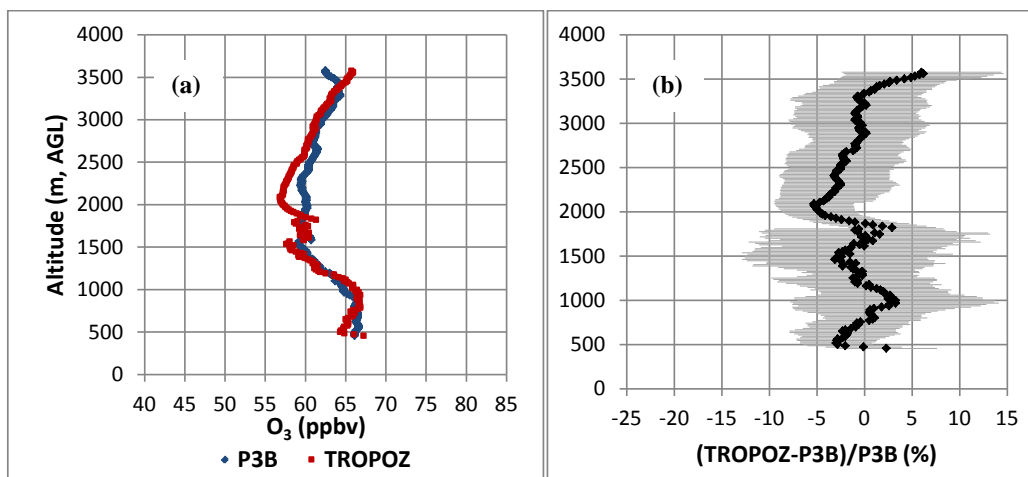
368 Figure 3. Comparisons of lidar and ozonesonde measurements. (a) Average ozone profiles measured by TROPOZ and
369 ozonesondes at Fort Collins, CO (11 pairs). (b) Mean relative difference between TROPOZ and ozonesondes as well as the
370 1- σ standard deviations. (c) Average ozone profiles measured by TOPAZ and ozonesondes at BAO Tower (7 pairs). (d)
371 Mean relative difference between TOPAZ and ozonesondes. (e) Average ozone profiles measured by LMOL and
372 ozonesonde at the BAO tower (1 pair). (f) Relative difference between LMOL and ozonesonde.

373

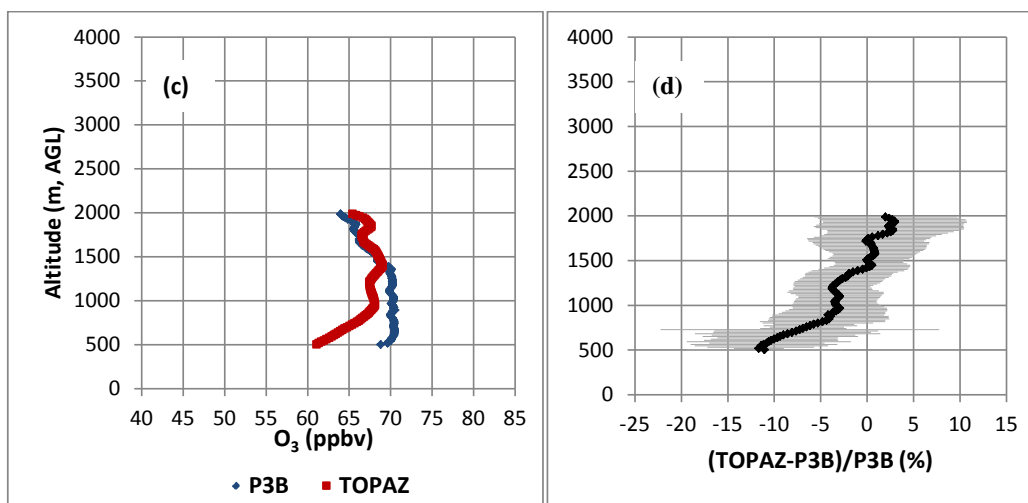
374



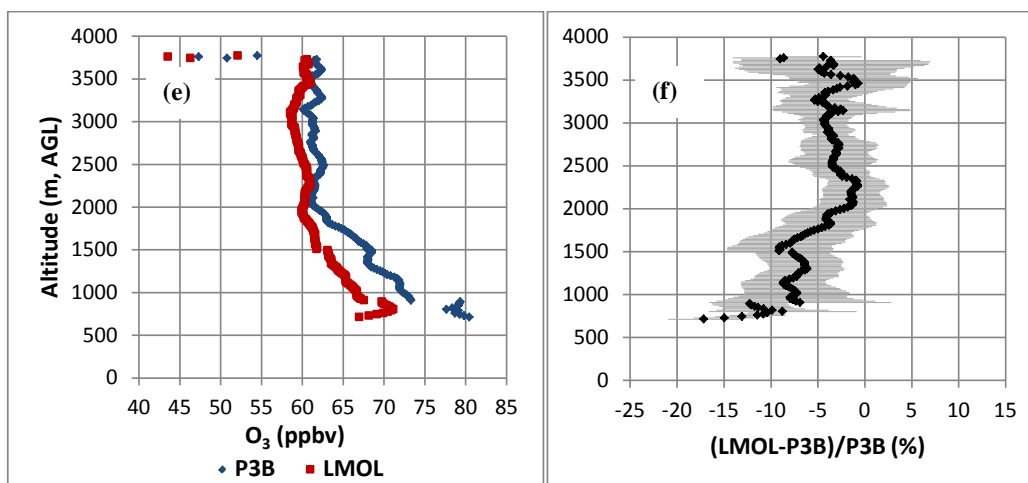
375



376



377





378 (e) (f)
 379 **Figure 4. Intercomparison between the lidar and P-3B measurements. (a) Average ozone profiles measured by TROPOZ**
 380 **and P-3B at Fort Collins, CO (34 profiles). (b) Mean relative difference between TROPOZ and P-3B data as well as the 1-**
 381 **σ standard deviation. (c) Average ozone profiles measured by TOPAZ and P-3B at the BAO Tower (29 profiles). (d) Mean**
 382 **relative difference between TOPAZ and P-3B data. (e) Average ozone profiles measured by LMOL and P-3B at Golden,**
 383 **CO (9 profiles). (f) Mean relative difference between LMOL and P-3B data.**

384

385

386

References

387

388

389

390

391

392

393

394

395

396

397

398

399

400

401

402

403

404

405

406

407

408

409

410

411

412

413

414

415

416

417

418

419

420

421

422

423

424

425

426

427

428

429

430

- Alvarez, R. J., Senff, C. J., Langford, A. O., Weickmann, A. M., Law, D. C., Machol, J. L., Merritt, D. A., Marchbanks, R. D., Sandberg, S. P., Brewer, W. A., Hardesty, R. M., and Banta, R. M.: Development and Application of a Compact, Tunable, Solid-State Airborne Ozone Lidar System for Boundary Layer Profiling, *J. Atmos. Oceanic Tech.*, 28, 1258-1272, 10.1175/JTECH-D-10-05044.1, 2011.
- Bowman, K. W.: Toward the next generation of air quality monitoring: Ozone. *Atmos. Environ.*, 80, 571-583, 2013.
- Brion, J., Chakir, A., Daumont, D., and Malicet, J.: High-resolution laboratory absorption cross section of O₃ temperature effect, *Chem. Phys. Lett.*, 213, 510-512, 1993.
- Browell, E. V., Ismail, S., and Shipley, S. T.: Ultraviolet DIAL measurements of O₃ profiles in regions of spatially inhomogeneous aerosols, *Appl. Opt.*, 24, 2827-2836, 1985.
- Crawford, J. H., and Pickering, K. E.: DISCOVER-AQ: Advancing strategies for air quality observations in the next decade, *Environ. Manage.*, 4-7, 2014.
- Daumont, D., Brion, J., Charbonnier, J., and Malicet, J.: Ozone UV spectroscopy I: Absorption cross-sections at room temperature, *J. Atmos. Chem.*, 15, 145-155, 1992.
- De Young, R., Carrion, W., Ganoe, R., Pliutau, D., Gronoff, G., Berkoff, T., and Kuang, S.: Langley mobile ozone lidar: ozone and aerosol atmospheric profiling for air quality research, *Appl. Opt.*, 56, 721, 10.1364/ao.56.000721, 2017.
- Deshler, T., Mercer, J. L., Smit, H. G. J., Stubi, R., Levrat, G., Johnson, B. J., Oltmans, S. J., Kivi, R., Thompson, A. M., Witte, J., Davies, J., Schmidlin, F. J., Brothers, G., and Sasaki, T.: Atmospheric comparison of electrochemical cell ozonesondes from different manufacturers, and with different cathode solution strengths: The balloon experiment on standards for ozonesondes., *J. Geophys. Res.*, 113, D04307, doi: 10.1029/2007/JD008975, 2008.
- Dingle, J. H., Vu, K., Bahreini, R., Apel, E. C., Campos, T. L., Flocke, F., Fried, A., Herndon, S., Hills, A. J., Hornbrook, R. S., Huey, G., Kaser, L., Montzka, D. D., Nowak, J. B., Reeves, M., Richter, D., Roscioli, J. R., Shertz, S., Stell, M., Tanner, D., Tyndall, G., Walega, J., Weibring, P., and Weinheimer, A.: Aerosol optical extinction during the Front Range Air Pollution and Photochemistry Experiment (FRAPPÉ) 2014 summertime field campaign, Colorado, USA, *Atmos. Chem. Phys.*, 16, 207-217, doi:10.5194/acp-16-11207-2016, 2016.
- Eisele, H., and Trickl, T.: Improvements of aerosol algorithm in ozone lidar data processing by use of evolutionary strategies, *Appl. Opt.*, 44, 2638-2651, 2005.
- Gaudel, A., Ancellet, G. and Godin-Beekmann, S.: Analysis of 20 years of tropospheric ozone vertical profiles by lidar and ECC at Observatoire de Haute Provence (OHP) at 44 N, 6.7 E, *Atmos. Environ.*, 113, 78-89, 2015.
- Godin, S. M., Carswell, A. I., Donovan, D. P., Claude, H., Steinbrecht, W., McDermid, I. S., McGee, T. J., Gross, M. R., Nakane, H., Swart, D. P. J., Bergwerff, H. B., Uchino, O., Gathen, P. v. d., and Neuber, R.: Ozone differential absorption lidar algorithm intercomparison, *Appl. Opt.*, 38, 6225-6236, 1999.
- Immler, F.: A new algorithm for simultaneous ozone and aerosol retrieval from tropospheric DIAL measurements, *Appl. Phys. B*, 76, 593-596, 2003.
- Johnson, B. J., Helmig, D., and Oltmans, S.: Evaluation of ozone measurements from a tethered balloon-sampling platform at South Pole Station in December 2003, *Atmos. Environ.*, 42, 2780-2878, 10.1016/j.atmosenv.2007.03.043, 2008.
- Komhyr, W. D.: Electrochemical cells for gas analysis, *Ann. Geophys.*, 25, 203-210, 1969.
- Komhyr, W. D., Barnes, R. A., Brothers, G. B., Lanthrop, J. A., and Opperman, D. P.: Electrochemical concentration cell ozonesonde performance evaluation during STOIC 1989, *J. Geophys. Res.*, 100, 9231-9244, 1995.



- 431 Kovalev, V. A., and Bristow, M. P.: Compensational three-wavelength differential-absorption lidar technique for
 432 reducing the influence of differential scattering on ozone-concentration measurements, *Appl. Opt.*, 35,
 433 4790-4797, 1996.
- 434 Kuang, S., Burris, J. F., Newchurch, M. J., Johnson, S., and Long, S.: Differential Absorption Lidar to Measure
 435 Subhourly Variation of Tropospheric Ozone Profiles, *IEEE Transactions on Geoscience and Remote
 436 Sensing*, 49, 557-571, 10.1109/TGRS.2010.2054834, 2011.
- 437 Kuang, S., Newchurch, M. J., Burris, J., and Liu, X.: Ground-based lidar for atmospheric boundary layer ozone
 438 measurements, *Appl. Opt.*, 52, 3557-3566, 10.1364/AO.52.003557, 2013.
- 439 Langford, A. O., Senff, C. J., Alvarez II, R. J., Banta, R. M., Hardesty, M., Parrish, D. D., and Ryerson, T. B.:
 440 Comparison between the TOPAZ airborne ozone lidar and in situ measurements during TexAQS 2006, *J.
 441 Atmos. Oceanic Technol.*, 28, 1243-1257, doi: <http://dx.doi.org/10.1175/JTECH-D-10-05043.1> 2011.
- 442 Langford, A. O., Alvarez, R. J., Brioude, J., Fine, R., Gustin, M., Lin, M. Y., Marchbanks, R. D., Pierce, R. B.,
 443 Sandberg, S. P., Senff, C. J., Weickmann, A. M., and Williams, E. J.: Entrainment of stratospheric air and
 444 Asian pollution by the convective boundary layer in the Southwestern U.S, *Journal of Geophysical
 445 Research: Atmospheres*, n/a-n/a, 10.1002/2016JD025987, 2016.
- 446 Leblanc, T., Sica, R. J., van Gijssel, J. A. E., Godin-Beekmann, S., Haefele, A., Trickl, T., Payen, G., and Gabarrot,
 447 F.: Proposed standardized definitions for vertical resolution and uncertainty in the NDACC lidar ozone and
 448 temperature algorithms – Part 1: Vertical resolution, *Atmos. Meas. Tech.*, 9, 4029-4049, 10.5194/amt-9-
 449 4029-2016, 2016.
- 450 Liu, G., Tarasick, D. W., Fioletov, V. E., Sioris, C. E. and Rochon, Y. J.: Ozone correlation lengths and
 451 measurement uncertainties from analysis of historical ozonesonde data in North America and Europe. *J. of
 452 Geophys. Res.*, 114, D04112, 2009.
- 453 Liu, X., Bhartia, P. K., Chance, K., Spurr, R. J. D., and Kurosu, T. P.: Ozone profile retrievals from the Ozone
 454 Monitoring Instrument, *Atmos. Chem. Phys.*, 10, 2521-2537, 2010.
- 455 Malicet, C., Daumont, D., Charbonnier, J., Parisse, C., Chakir, A., and Brion, J.: Ozone UV spectroscopy. II.
 456 Absorption cross-sections and temperature dependence, *J. Atmos. Chem.*, 21, 263-273, 1995.
- 457 McDermid, I. S., Godin, S. M., Lindqvist, L. O., Walsh, T. D., Burris, J., Butler, J., Ferrare, R., Whiteman, D., and
 458 McGee, T. J.: Measurement intercomparison of the JPL and GSFC stratospheric ozone lidar systems, *Appl.
 459 Opt.*, 29, 4671-4676, 1990.
- 460 Newchurch, M. J., Kuang, S., Leblanc, T., Alvarez, R. J., Langford, A. O., Senff, C. J., Burris, J. F., McGee, T. J.,
 461 Sullivan, J. T., DeYoung, R. J., and Al-Saadi, J.: TOLNET - A Tropospheric Ozone Lidar Profiling
 462 Network for Satellite Continuity and Process Studies, *The 27th International Laser Radar Conference
 463 (ILRC 27)*, 2016,
- 464 Papayannis, A., Ancellet, G., Pelon, J., and Mégie, G.: Multiwavelength lidar for ozone measurements in the
 465 troposphere and the lower stratosphere, *Appl. Opt.*, 29, 467-476, 1990.
- 466 Ridley, B. A., Grahek, F. E., and Walega, J. G.: A small high-sensitivity, medium-response ozone detector suitable
 467 for measurements from light aircraft, *J. Atmos. Oceanic Technol.*, 9, 142-148, 1992.
- 468 Senff, C. J., Alvarez, R. J., Hardesty, R. M., Banta, R. M., and Langford, A. O.: Airborne lidar measurements of
 469 ozone flux downwind of Houston and Dallas, *J. Geophys. Res.: Atmospheres*, 115, n/a-n/a,
 470 10.1029/2009JD013689, 2010.
- 471 Smit, H. G. J., Straeter, W., Johnson, B. J., Oltmans, S. J., Davies, J., Tarasick, D. W., Hoegger, B., Stubi, R.,
 472 Schmidlin, F. J., Northam, T., Thompson, A. M., Witte, J. C., Boyd, I., and Posny, F.: Assessment of the
 473 performance of ECC-ozonesondes under quasi-flight conditions in the environmental simulation chamber:
 474 Insights from the Juelich Ozone Sonde Intercomparison Experiment (JOSIE), *J. Geophys. Res.*, 112,
 475 D19306, doi:10.1029/2006JD007308, 2007.
- 476 Stauffer, R. M., Morris, G. A., Thompson, A. M., Joseph, E., Coetzee, G. J. and Nalli, N. R.: Propagation of
 477 radiosonde pressure sensor errors to ozonesonde measurements, *Atmos. Meas. Tech.*, 7, 65-79, 2014.
- 478 Steinbrecht, W., McGee, T. J., Twigg, L. W., Claude, H., Schönnenborn, F., Sumnicht, G. K., and Silbert, D.:
 479 Intercomparison of stratospheric ozone and temperature profiles during the October 2005 Hohenpeißenberg
 480 Ozone Profiling Experiment (HOPE), *Atmos. Meas. Tech.*, 2, 125-145, 2009.
- 481 Sullivan, J. T., McGee, T. J., Sumnicht, G. K., Twigg, L. W., and Hoff, R. M.: A mobile differential absorption lidar
 482 to measure sub-hourly fluctuation of tropospheric ozone profiles in the Baltimore-Washington, D.C. region,
 483 *Atmos. Meas. Tech.*, 7, 3529-3548, 10.5194/amt-7-3529-2014, 2014.
- 484 Sullivan, J. T., McGee, T. J., DeYoung, R., Twigg, L. W., Sumnicht, G. K., Pliutau, D., Knepp, T., and Carrion, W.:
 485 Results from the NASA GSFC and LaRC Ozone Lidar Intercomparison: New Mobile Tools for
 486 Atmospheric Research, *J. Atmos. Oceanic Technol.*, 32, 1779-1795, doi:10.1175/JTECH-D-14-00193.1, 2015.



487 Weinheimer, A. J., Walega, J. G., Ridley, B. A., Satche, G. W., Anderson, B. E., and Collins Jr., J. E.: Stratospheric
488 NO_y measurements on the NASA DC-8 during AASE II, Geophys. Res. Lett., 20, 2563-2566, 1993.
489